Computational Materials Science 166 (2019) 303–310

Contents lists available at ScienceDirect

Computational Materials Science

journal homepage: www.elsevier.com/locate/commatsci

Novel high/ultrahigh pressure structures of TiO_2 with low band gaps

D. Bedghiou[a,b,c,*], F. Hamza Reguig[b], A. Boumaza[c]

[a] Structures, Properties and InterAtomic Interactions Laboratory (LASPI²A), University of Abbès Laghrour, 40000 Khenchela, Algeria
[b] Macromolecular Chemistry and Physics Laboratory (LCPM), University Oran 1 Ahmed Ben Bella, 31000 Oran, Algeria
[c] Chemistry and Physics of Biomolecules Laboratory (CPB), University of Namur, B-5000 Namur, Belgium

ARTICLE INFO

Keywords:
Rutile TiO_2
Band gap
High/ultrahigh pressure
Crystal structure prediction

ABSTRACT

The high photoactivity of titanium dioxide at UV region has attracted ample attention over recent. The present work aims to predict highly photoactive TiO_2 crystal structures under high/ultrahigh pressure (up 300 GPa). Global minimizations of rutile TiO_2 band gap were performed using first-principles calculations combined with the evolutionary algorithm USPEX (Universal Structure Prediction: Evolutionary Xtallography). Among several phases predicted, three semiconductors with low band gaps were selected to study their structural, thermodynamic, dynamical, and electronic properties. These phases show new symmetry (P4/nmm), coordination number up to nine, and the lowest enthalpy of formation values (until −9.27 eV) ever reported to TiO_2 compounds. In order to confirm the USPEX efficiency, a comparison between band gaps obtained by GGA, GGA + U, and HSE06 calculations was performed. Relative stability and bulk modulus of dynamically stable phases are also investigated. Finally, our calculations reveal that R-semiconductor-300 exhibits the lowest direct band gap predicted for TiO_2 to date.

1. Introduction

In solid-state physics, electronic band theory classifies materials based on their own energy band structure into four main categories: metals, insulators, semiconductors, and semimetals. In the case of metals, the fermi energy (E_F) crosses through at least one band, which means that the valence band overlaps the conduction band. In insulators the valence and conduction bands are separated by a large gap ($E_g > 4$ eV), whereas there is a small gap in semiconductors ($0 < E_g < 4$ eV). Semimetals are semiconductors with a negative indirect bandgap [1]. As a result of its high activity under UV irradiation, TiO_2 has been the most studied semiconductor photocatalyst [2]. It has also attracted a great deal of attention because of its outstanding physical properties [3–11], which shows a rich structural phase diagram including many polymorphs [12–14], among them the three common phases rutile ($P4_2/mnm$, D_{4h}^{14}) [15,16], anatase ($I4_1/amd$, D_{4h}^{19}) [17,18], and brookite (OI, Pbca, D_{2h}^{15}) [19,20] are mainly found in nature [21].

Rutile has been well explored due to its versatile physical and chemical properties, especially its high stability [22], its crystal structure has been determined with lattice parameters a = 4.5937 Å and c = 2.9581 Å [21]. Several studies have revealed that rutile has a direct band gap of 3.06 eV and an indirect one of 3.10 eV [23]. It is obvious that the band-edge positions (conduction band and valence band) of TiO_2 photocatalyst play a crucial role in the capture of solar energy [24–26]. Therefore, semiconductor material should have a smaller band gap to increasing the visible light absorption, which enhances its photocatalytic activity [2].

Studying the properties of condensed matter subjected to very high pressures describes efficiently their behaviour under extreme conditions. Compression of solids leads atoms to bring closer, causing an increase in the overlap of electronic orbitals and inducing modifications in the nature of chemical bonds and electronic band structure. These changes push the materials to undergo new transitions as the modifications occurring continuously or discontinuously create new different physical and structural properties [27]. Studying these changes in extreme conditions provides understanding the nature of phase transformations [28], crystal to amorphous transitions [29], chemical changes [30], valence transitions [31] as good as changes in the dielectric function [32].

An enormous amount of research has indicated that the compression can manipulate effectively the electronic properties of materials, through which the insulator-to-metal [33], metal-to-semiconductor [34,35], semiconductor-to-semimetal [36] or metal-to-semimetal transition [37] takes place.

In this paper, we predict possible crystal polymorphs of TiO_2 with low band gap at high/ultrahigh pressures (up 300GPa) using

* Corresponding author at: Structures, Properties and InterAtomic Interactions Laboratory (LASPI2A), University of Abbès Laghrour, 40000 Khenchela, Algeria. Tel.: +213 7 94 54 60 41.
E-mail address: Djohrachimiste@outlook.fr (D. Bedghiou).

https://doi.org/10.1016/j.commatsci.2019.05.016
Received 13 December 2018; Received in revised form 6 May 2019; Accepted 7 May 2019

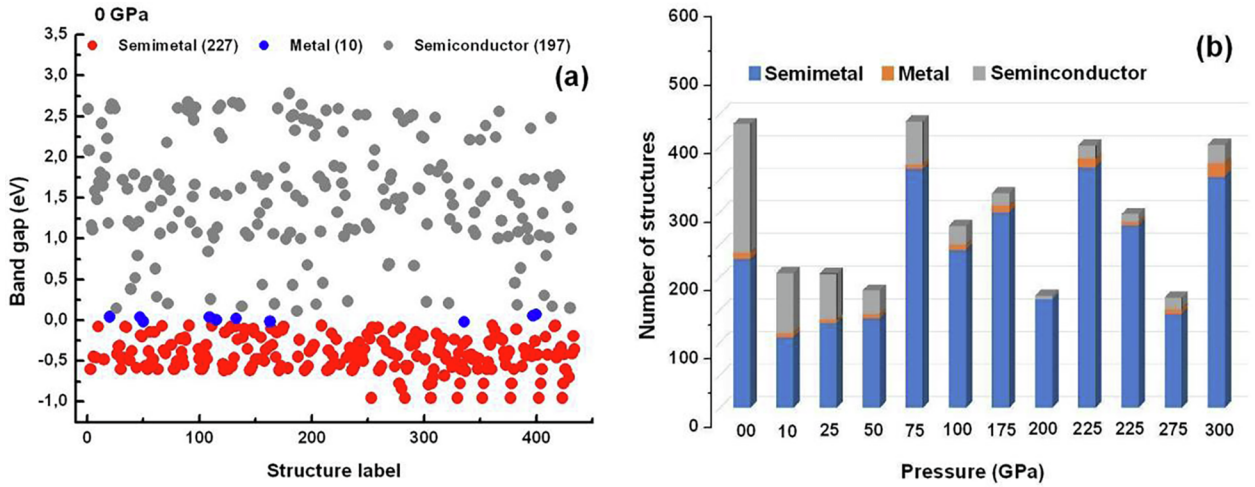

Fig. 1. (a) Example of evolutionary band gap minimization: an *ab initio* run for rutile; (b) histogram of number of structures predicted at each pressure.

evolutionary algorithm USPEX (Universal Structure Prediction: Evolutionary Xtallography), which operates with populations of structures. From parent structures, new population is produced according to its fitness rank (enthalpy by default) using one of three operators: heredity, permutation or mutation. After that, the locally optimal structure having lowest-enthalpy is selected for producing structures of the next generation, and so on until reaching a sufficient number of new structures. By the way, energy calculations and local optimization are done by external codes interfaced with USPEX (usually, VASP [38], SIESTA [39] or GULP [40]) [41]. This method demonstrated a remarkable, nearly 100%, success rate when it was applied on several dozen compounds with well-known structures [42].

2. Theoretical methods

Our approach is based on the evolutionary algorithm USPEX [43–47], the fitness function was chosen to be the band gap instead of the free energy. In our case, a candidate solution is a locally optimized with respect to the energy, rather than band gap, to ensure that the structure is chemically realistic. Afterwards, all bad candidates (their quality is determined by the value of the band gap) were eliminated [44].

Our structure prediction runs for TiO_2 were performed at high pressure (0, 10, 25, 50, 75, and 100 GPa) and ultrahigh pressure (175, 200, 225, 250, 275, and 300 GPa) all at zero Kelvin, and for systems containing 6 atoms/cell. The population size was in the range 15–20, typical structure prediction runs required ~10–25 generations. The first generation was produced randomly, whereas succeeding generations were obtained by applying heredity (50%), softmutation (20%), and latmutation (10%) operations, while 20% of each generation was produced using symmetric random generator.

In this study, evolutionary searches were achieved with local optimization using density functional theory (DFT) [48,49] within the spin-polarized GGA-PBE functional [50], and the projector-augmented wave method [51,52], as implemented in the VASP software [52–54], plane wave kinetic energy cutoff was set to 320 eV. All ab initio calculations used plane-wave basis sets and Monkhorst-Pack meshes for Brillouin zone, sufficient for excellent convergence in the total energy, stress tensor, and bandgap.

The enthalpies of formation for the TiO_2 phases identified after each generation of the USPEX structure prediction run are also calculated. The enthalpy is given relative to the energy of the optimized elemental phases of Ti and O as follows:

$$\Delta H_f = E(Ti_xO_y) - [xE(Ti) + yE(O)]/(x + y) \quad (1)$$

where E stands for the total energy per atom of the phase, while x and y stand for the stoichiometric proportions of Ti and O, respectively [55], in TiO_2 phases (fixed-composition binary system), with x = 1 and y = 2.

On the other hand, according to the empirical Eq. (2) [56,57] we can define the band gap as follow:

$$E_{BI} = 1.36 \times \left(\frac{E_g}{E_{gc}}\right)^{\alpha}, \quad (2)$$

where, E_{BI}: intrinsic breakdown field (V nm^{-1}), E_g: band gap (eV), E_{gc} = 4.0 eV, and α = 3 for semiconductors, and α = 1 for insulators.

GGA is well known to underestimate the band gap by 10–40%, and more accurate values can be found by other methods such as: the GW approximation or hybrid functionals, but, here, DFT band gaps have used as approximate and useful guide values [58].

The dynamical stability was investigated by phonon calculations as implemented in the PHONOPY code [59]. Band structure and partial density of states (PDOS) have been performed using the CASTEP module [60] of Materials Studio, with generalized gradient approximation (GGA) and the screened hybrid functional by Heyd, Scuseria and Ernzerhof (HSE06). Crystal structures of best predicted phases are generated using VESTA [61] software (Fig. 3 and Fig. S3). Origin program was used to create the artwork [62].

3. Results and discussion

3.1. Statistical aspects of simulation results

A typical evolutionary prediction of TiO_2 low band gap structures using the rutile experimental cell parameters (6 atoms/cell) at 0 GPa is shown in Fig. 1(a), similar simulations were also run at high pressure (10, 25, 50, 75, and 100 GPa) and ultrahigh pressure (175, 200, 225, 250, 275, and 300 GPa) as displayed in Fig. S1. The histogram plots in Fig. 1(b) recapitulate the number of structures predicted at each pressure, it is remarkable that compression leads to semiconductor-to-metal, metal-to-semimetal or semiconductor-to-semimetal reversible transition in rutile due to the reduction of interatomic distances and strengthening of interatomic interactions. This is well in line with published results [29,35,36,63], where rutile tends generally to become a semimetal, especially at ultrahigh pressure. Our searches at various pressures (in total, we sampled 3505 structures) produced a large number of allotropes with low band gap, knowing that rutile is most/lowest transformable at 75 GPa (437 structures) and 275 GPa (168 structures) respectively. Besides, the band gap values recorded in this work ranging from −1.09 eV predicted at 275 GPa to 2.89 eV at 10 GPa.

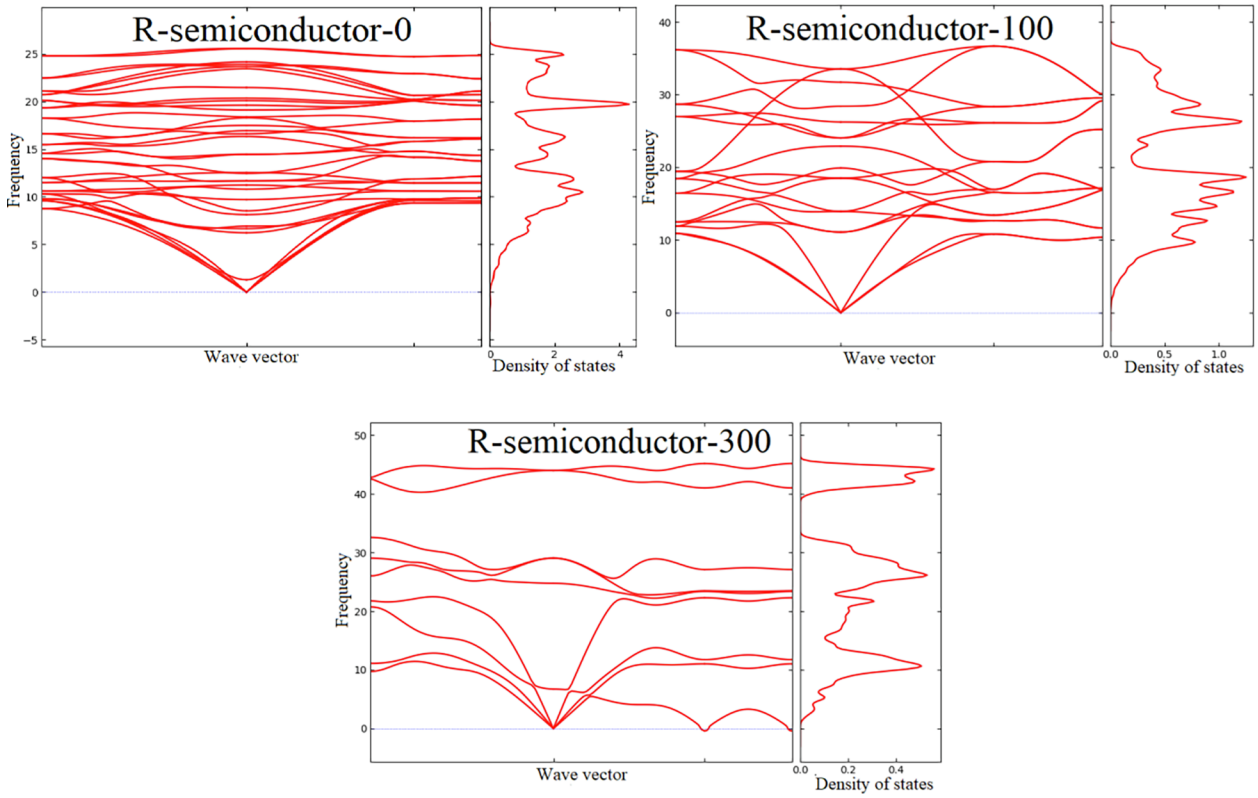

Fig. 2. The phonon band structure and phonon DOS charts for stable R-semiconductors.

3.2. Structural and thermodynamic properties

In order to facilitate the representation of the new compounds predicted in this study, we have named them as follow: Initial letter-Type-Pressure. The first part of the name (Initial letter) is simply the initial name of TiO_2 parent structure, the second part (Type) represents the nature of the new structure, *i.e.*, semimetal, metal or semiconductor, while the last part (Pressure) is the applied pressure (GPa). For example: R-semiconductor-0 denotes the lowest band gap semiconductor produced from rutile at 0 GPa.

Our phonon computations (Fig. 2) for R-semiconductor-0, R-semiconductor-100, and R-semiconductor-300 did not reveal any imaginary frequencies confirming that these structures are minima, while all the rest of the semiconductors illustrated in Fig. S2 is dynamically unstable.

The crystal structures of the stable lowest band gap semiconductors are depicted in Fig. 3, their calculated structural parameters, their gaps and their enthalpies of formation are displayed in Table 1. More information about metastable lowest band gap semiconductors are available in Fig. S3 and Table S1.

Our results show that rutile could crystallize in C2/m (at 0 GPa) and P3m1 (at 300 GPa) space groups. This is the first report, to our knowledge, of the pressure-induced phase transition to P4/nmm (at 100 GPa) structure among all titanate compounds. For R-semiconductor-0, O atoms form an irregular hendecahedron (Polyhedral volume = 14.52 $Å^3$) with Ti atoms sitting at the 4i (0.320, 0.000, 0.278) Wyckoff site, and O atoms sitting at the 4i (−0.344, 0.000, 0.063) and 4i (−0.086, 0.000, −0.387) Wyckoff sites. In R-semiconductor-100, and R-semiconductor-300, O atoms built a distorted polyhedron with polyhedral volume = 15.03 $Å^3$, and 12.89 $Å^3$ respectively. The cation occupying 2c (0.250, 0.250, 0.248) site while the anions are at 2a (0.750, 0.250, 0.000) and 2c (0.250, 0.250, −0.367) sites in R-semiconductor-100, however, Ti ions are at 1a (0.000, 0.000, 0.209) and O ions occupying 1c (0.666, 0.333, 0.181) and 1b (0.333, 0.666, −0.291) in R-semiconductor-300. In both R-semiconductor-100 and R-semiconductor-300, each Ti is coordinated to nine O ions with Ti-O average bond length estimated to 1.94 Å and 1.880 Å respectively. R-

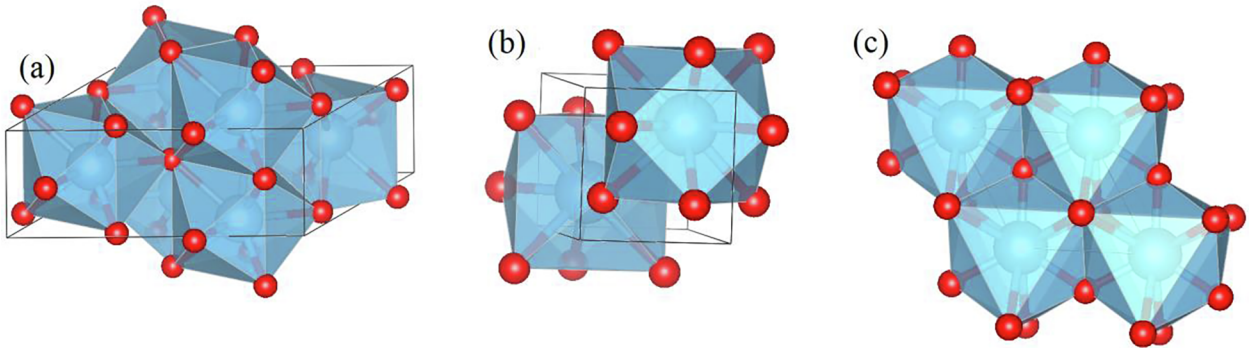

Fig. 3. Polyhedra structures for stable TiO_2 semiconductors: (a) R-semiconductor-0, (b) R-semiconductor-100, and (c) R-semiconductor-300. Blue atoms depict Ti, while red atoms present O.

Table 1
Details of crystal structure of R-semiconductors.

TiO_2 structure	Space group (No.)	Structure parameters (Å, °)	Wyckoff positions	Enthalpy of formation (eV/atom)	Bandgap E_g (eV)
R-semiconductor-0	C2/m (12)	a = 7.21, b = 2.73, c = 5.41, β = 119	Ti 4i (0.320, 0.000, 0.278), O1 4i (−0.344, 0.000, 0.063), O2 4i (−0.086, 0.000, −0.387)	−9.27	0.11
R-semiconductor-100	P4/nmm (1 2 9)	a = 2.81, b = 2.81, c = 4.81	Ti 2c (0.250, 0.250, 0.248), O1 2a (0.750, 0.250, 0.000), O2 2c (0.250, 0.250, −0.367)	−4.86	0.21
R-semiconductor-300	P3m1 (1 5 6)	a = 2.89, b = 2.89, c = 2.12	Ti 1a (0.000, 0.000, 0.209), O1 1c (0.666, 0.333, 0.181), O2 1b (0.333, 0.666, −0.291)	+3.61	0.11

semiconductor-0 has coordination number of eight with Ti-O average distance of 2.02 Å.

By the way, the predicted favoured structure of TiO_2 is C2/m with $a = 7.21$ Å, $b = 2.73$ Å, and $c = 5.41$ Å, that is quite far to the known C2/m TiO_2 lattice parameters, *i.e.*, TiO_2-(B) [64] with a = 12.30 Å, b = 3.76 Å and c = 6.61 Å and another C2/m [65] structure with a = 14.26 Å, b = 2.98 Å and c = 4.78 Å. Therefore, this major difference in C2/m structures, which caused especially by compression along *a*direction, leads to intrinsic variation in band gap values from $E_g = 2.6\ eV$ [64] in the case of TiO_2-(B) and $E_g = 2.1\ eV$ [65] for the second C2/m structure to $E_g = 0.1\ eV$ in our structure.

Likewise, a new phase of TiO_2 with P3m1 symmetry were predicted using density functional theory (DFT) [65]. Its unit cell has the following lattice parameters: a = 6.02 Å, b = 6.02Å, and c = 14.78 Å. However, from our calculations, R-semiconductor-300 has a P3m1 symmetry and lattice vectors a = 2.89 Å, b = 2.89 Å, and c = 2.12 Å. Despite the fact that these two phases have the same symmetry, their structures are rather dissimilar with largely various band gap values, *i.e.*, E_g (P3m1) = 1.73 eV (using GGA) [65] and E_g (R-semiconductor-300) = 0.11 eV.

A few years ago, the Fe_2P-type (P62m) structure predicted at 210 GPa, which was considered as the highest-pressure phase of TiO_2, was found to have the highest coordination number (ninefold) among the known TiO_2 polymorphs [66]. However, a ten-coordinated TiO_2 structure with space group I4/mmm (CaC_2-type) was recently discovered above 650–690 GPa, knowing that significant differences in the electronic properties between Fe_2P-type and CaC_2-type structures were found [67,68]. In this study, R-semiconductors have coordination number of six at 10 GPa, seven at 25 and 50 GPa, eight at 0 GPa, nine at 75, 100 and 300 GPa, and ten at 175–275 GPa. J. Muscat et al. [69] found that O ions are more compressible than Ti ions at high pressure, such that it is possible to form more anions around each cation hence increasing the Ti-O attraction interaction. This leads to an increase in the coordination of Ti-O ions from six (R-semiconductor-10) to ten (R-semiconductor-275).

On the other hand, the current calculations demonstrate that high pressure semiconductors are characterized by lower coordination number and higher band gap ($E_{g\ moy} = 0.13\ eV$) compared with ultra-high pressure semiconductors, which have higher coordination number and lower band gap ($E_{g\ moy} = 0.12\ eV$). Subsequently, band gap decreases generally with coordination number because of decreasing bond strength which leads to increasing the dielectric constant. These results are in excellent agreement with recent results obtained by theoretical computation [58].

We have investigated also the change in the unit cell parameters of R-semiconductors (see Fig. 4(a)), we have observed that the freedom of movement of Ti ions along the c direction makes it the most compressible direction, while the three directions tend to resist compression from 175 GPa to 275 GPa. Fig. 4(b) portrays the evolution of the average polyhedral Ti-O, the nearest Ti-Ti, and O-O bond distances. Clearly, the change in Ti-Ti and O-O bond lengths is not evident due to the free movement of the nearest Ti and O ions in order to rearranging the polyhedron, whereas Ti-O bond distances are so similar.

Analysing our enthalpy of formation results, we note that only R-semiconductor-300 is thermodynamically unstable. Besides that, R-semiconductor-0 and R-semiconductor-100 are newly predicted structures with highly lower enthalpies (−9.27 and −4.86 eV/atom respectively) compared to the formation energy values of the 39 known stable polymorphs of TiO_2, which range from −3.52 to −0.80 eV/atom [65].

3.3. Relative stability

We have used BFGS algorithm [70] to perform geometry optimization for rutile TiO_2, R-semiconductor-0, R-semiconductor-100, and R-semiconductor-300. The equilibrium volume V_0, bulk modulus B_0 and its first derivative $B_0^{'}$ were calculated through Birch Murnaghan equation (3) of state [71] as presented below, for all phases, cell optimizations were done for fifteen different pressures.

$$P(V) = \frac{3B_0}{2}\left[\left(\frac{V_0}{V}\right)^{\frac{7}{3}} - \left(\frac{V_0}{V}\right)^{\frac{5}{3}}\right]\left\{1 + \frac{3}{4}(B_0^{'} - 4)\left[\left(\frac{V_0}{V}\right)^{\frac{2}{3}} - 1\right]\right\}, \quad (3)$$

Predicted equilibrium volume of rutile 62.90 $Å^3$, bulk modulus 215 GPa and its pressure derivative 4.39, as listed in Table 2, are consistent with the recent high-pressure experiments [72,73] and first-principles calculations [74,75]. R-semiconductor-0 and R-semiconductor-100 exhibit lower bulk modulus (51, 41 GPa respectively) compared to rutile, which means that these new structures are less hard than rutile. According to R-semiconductor-300's bulk modulus (212 GPa), we can say that R-semiconductor-300 is as hard as rutile.

Moreover, we can deduce the transition pressures of crystal phase by determining the enthalpies of rutile, R-semiconductor-0, R-semiconductor-100, and R-semiconductor-300 under hydrostatic pressure from 0 to 300 GPa as illustrated in Fig. 5. The most stable structure at ambient conditions is rutile, where the enthalpy of R-semiconductor-0 is lower than that of both R-semiconductor-100 and R-semiconductor-300. The first phase transition, which corresponds to the R-semiconductor-100 to R-semiconductor-0 transformation, occurs about 15.62 GPa. Under increasing pressure, R-semiconductor-100, R-semiconductor-0, and R-semiconductor-300 convert to rutile at 38.52, 64.93, and 114.30 GPa, respectively. Above 38.52 GPa R-semiconductor-100 becomes the most stable phase. Remarkably, these predicted transformations are in stark contrast to USPEX results, this difference may be due to the sensitivity of relative stability calculations to the treatment of electronic exchange and correlation [17] and to the numerical details of the calculations [76].

3.4. Electronic properties

In order to establish the validity of band gap values found by USPEX for the semiconductors selected in this work, we have calculated the band energies at high symmetry k-points using GGA-PBE, GGA + U, and HSE06 functionals. M. E. Arroyo-de Dompablo et al. [77] found that the DFT + U (U ≈ 5 eV) method is well suitable to investigate the properties of TiO_2 polymorphs. For easy comparison, Fig. 6 depicts the

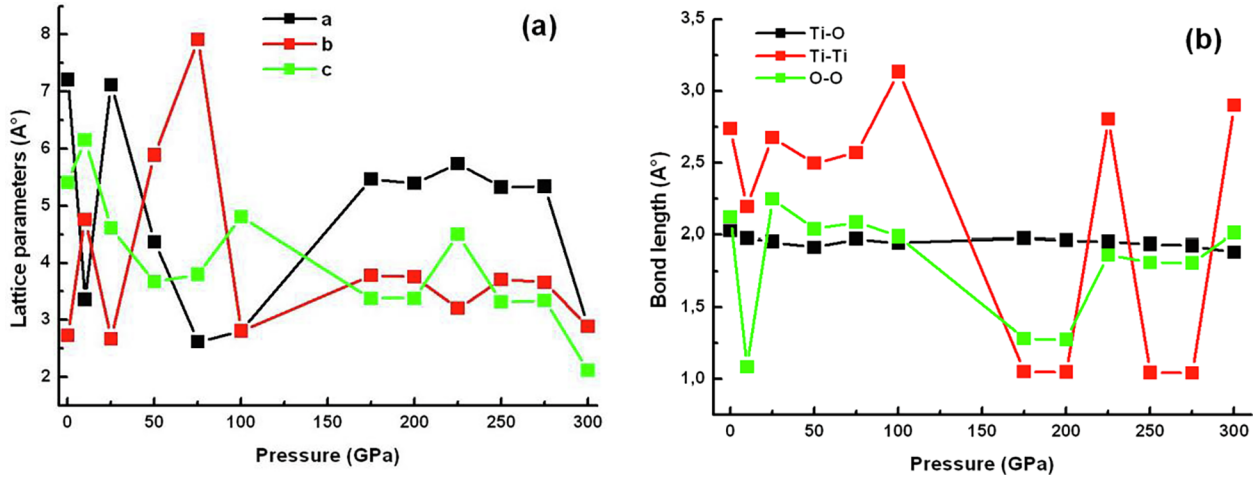

Fig. 4. (a) Pressure dependence of the lattice parameters of R-semiconductors; (b) The change in Ti-O, Ti-Ti, and O-O with pressure for R-semiconductors.

Table 2
Equilibrium volumes V_0 (Å^3/ two formula), bulk moduli B_0 (GPa), and first pressure derivative $B_0^{'}$ of rutile, R-semiconductor-0, R-semiconductor-100, and R-semiconductor-300 at 0 GPa.

Phase	Method	V_0 (Å^3)	B_0 (GPa)	$B_0^{'}$
Rutile	Present work	62.90	215	4.39
	Expt. [10,11]	62.00–62.44	211–235	6.84–4.00
	Other calc [12,13]	63.78–63.3	215–235	5.35–4
R-semiconductor-0	Present work	70.23	51	4.43
R-semiconductor-100	Present work	59.43	41	8.69
R-semiconductor-300	Present work	56.50	212	3.15

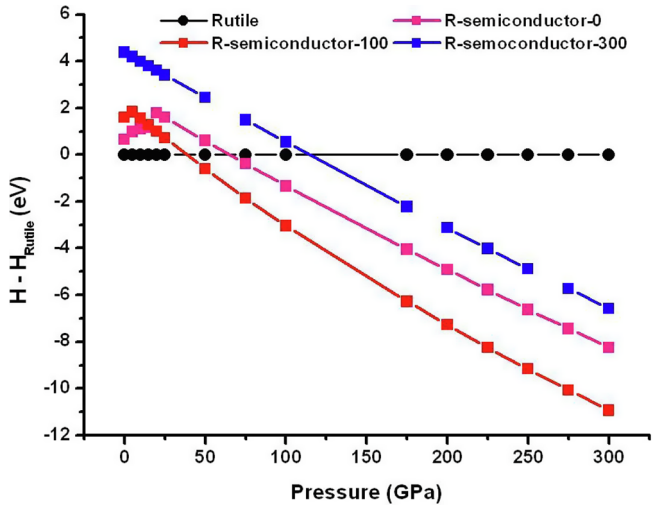

Fig. 5. Calculated enthalpy of R-semiconductor-0, R-semiconductor-100, and R-semiconductor-300 as a function of pressure, with the rutile phase as the reference state.

band gaps estimated using GGA, GGA + U, and HSE06. Comparing with band gap values predicted by USPEX ($E_g = 0.11\,eV$ at 0 GPa, $E_g = 0.21\,eV$ at 100 GPa, and $E_g = 0.11\,eV$ at 300 GPa), all of GGA, GGA + U, and HSE06 have overestimated them. Remarkably, within the GGA + U the optimization of the GGA band gaps is achieved at 0 GPa ($E_{g\,(GGA+U)} = 0.52\,eV$, $E_{g\,(GGA)}$=0, 30 eV), 100 GPa ($E_{g\,(GGA+U)} = 1.05\,eV$, $E_{g\,(GGA)}$=0, 93 eV), and at 300 GPa ($E_{g\,(GGA+U)} = 0.36\,eV$, $E_{g\,(GGA)} = 0.26\,eV$).We note that GGA + U method usually tends to underestimate the band gaps [77–79], however, the band gaps done by HSE06 are always overestimated. Thus, the

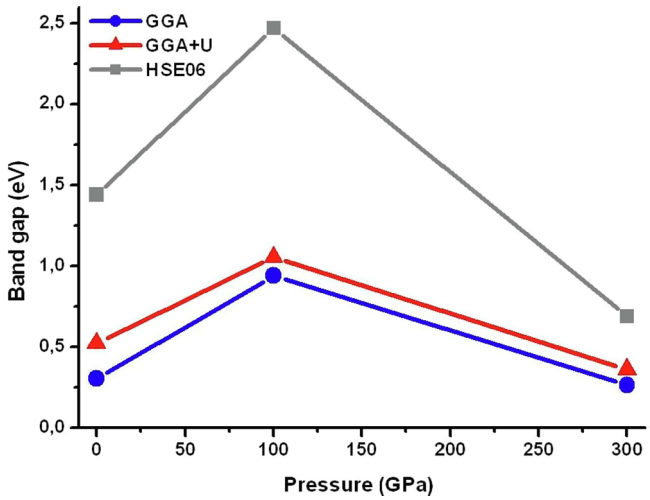

Fig. 6. Pressure dependence of the band gap of R-semiconductors at high/ultrahigh pressure obtained by GGA, GGA + U, and HSE06.

actual values should be confined between GGA + U and HSE06 values, which ensures that our structures really have low band gaps.

As an understanding of electronic properties of R-semiconductor-0, R-semiconductor-100, and R-semiconductor-300 is important to the work presented in this paper, we describe their band structures and densities of states in some detail (see Fig. 7). The HSE06 band structure of R-semiconductor-0 revealed that it has an indirect band gap of 1.44 eV with the VBM between Γ and F and the CBM at Z, however, an indirect band gap of 0.52 eV with the CBM at Γ was found by GGA + U calculation. For R-semiconductor-100, the HSE06 calculation yields an indirect band gap of 2.46 eV with the VBM between Z and Γ and the CBM at Γ, while GGA + U gives an indirect band gap of 1.05 eV with the VBM at Z and the CBM at Γ. From the HSE06 calculation, the minimum direct band gap for R-semiconductor-300 is 0.68 eV between Γ and F, the same band gap was found by GGA + U method but it was estimated to 0.36 eV. By the way, projected densities of states (PDOS) report that the three structures have dominant O 2*p* and Ti 3*d* orbitals in the valence and conduction bands, respectively.

Otherwise, the smallest band gap recorded for TiO_2 polymorphs belongs to Fe_2P-type structure, which is predicted at 160 GPa with $E_g = 0.66\,eV$ (GGA) [68]. Thus, R-semiconductor-300 shows the new lowest band gap predicted for titanium dioxide to date ($E_{g\,(GGA)}$=0.26 eV). In addition, DBG (direct band gap) semiconductors have generally high efficiency since no phonon assistance is needed for

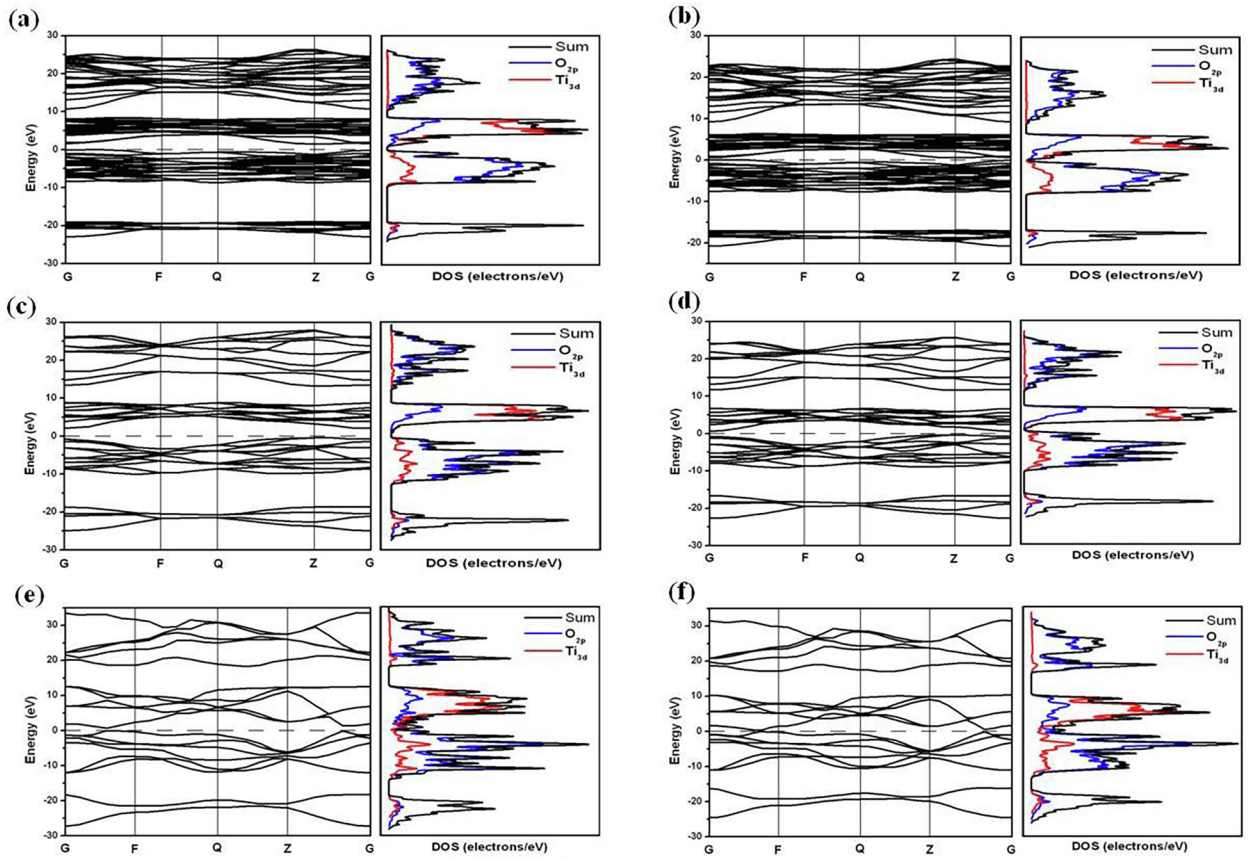

Fig. 7. Electronic band structures of: R-semiconductor-0 with (a) HSE06 and (b) GGA + U, R-semiconductor-100 with (c) HSE06 and (d) GGA + U, and R-semiconductor-300 with (e) HSE06 and (f) GGA + U. Horizontal black lines indicate the calculated Fermi energy (E_F). Electronic densities of states (electrons/eV), and their projections onto atomic orbitals, are also shown.

the minimum gap excitation [80]. Comparison to experimental/ theoretical data is not possible as equilibrated experiments/calculations at 0, 100, and 300 GPa, to our knowledge, have not yet been performed.

4. Conclusion and outlook

In summary, we have studied the structural, thermodynamic, dynamical, and electronic properties of new TiO_2 phases predicted by USPEX at high/ultrahigh pressure. Our results show that compression leads to reversible semiconductor-to-metal, metal-to-semimetal and semiconductor-to-semimetal transitions in rutile. Among twelve selected semiconductors with low band gaps, only R-semiconductor-0, R-semiconductor-100, and R-semiconductor-300 are dynamically stable. These new structures are characterized by highly lower enthalpies of formation (-9.27 eV/atom for R-semiconductor-0 and -4.86 eV/atom for R-semiconductor-100) and new recorded symmetry (P4/nmm) which belongs to R-semiconductor-100. We found also that under compression, R-semiconductor-100 transforms directly to R-semiconductor-0 at 15 GPa, and, upon release of pressure, R-semiconductor-100, R-semiconductor-0, and R-semiconductor-300 convert to rutile at 38, 65, and 114 GPa respectively, which are in contrast to USPEX predictions. Bulk modulus results suggest that R-semiconductor-0 and R-semiconductor-100 are softer than rutile, while R-semiconductor-300 is as hard as rutile. Otherwise, comparison between band gaps obtained by GGA, GGA + U, and HSE06 calculations yields: (i) all of GGA, GGA + U, and HSE06 overestimate the band gaps predicted by USPEX; (ii) USPEX has successfully discovered new TiO_2 phases with very low band gaps in spite of its negligence to dynamical stability aspects, which imposes certain fundamental issues. We present also, in this study, a new stable TiO_2 polymorph with the lowest direct band gap ever recorded for titanium dioxide ($E_g = 0.26\,eV$). Finally, understanding the high/ultrahigh pressure behaviour of new TiO_2 structures with low band gaps predicted from anatase and brookite, will be the subject of a forthcoming work.

CRediT authorship contribution statement

D. Bedghiou: Conceptualization, Methodology, Software, Formal analysis, Investigation, Data curation, Writing - original draft. **F. Hamza Reguig**: Software, Validation, Resources, Writing - review & editing, Supervision. **A. Boumaza**: Validation, Resources, Writing - review & editing, Visualization, Project administration, Funding acquisition.

Acknowledgment

This work was supported by Abbes Laghrour University of Khenchela, Ministry of Higher Education and Scientific Research (Algeria) and the University of Namur (Belgium). This research used resources of the “Plateforme Technologique de Calcul Intensif (PTCI)” (http://www.ptci.unamur.be) located at the University of Namur, Belgium, which is supported by the FNRS-FRFC, the Walloon Region, and the University of Namur (Conventions No. 2.5020.11, GEQ U.G006.15, 1610468 et RW/GEQ2016). The PTCI is member of the “Consortium des Équipements de Calcul Intensif (CÉCI)” (http://www.ceci-hpc.be). We are thankful to the High-Performance Computing Unity of University Oran 1 Ahmed Ben Bella who provided expertise that greatly assisted the research. We would like to thank Frédéric Wautelet (HPC System Administrator at University of Namur) for the hard work that he has done to have our calculations run.

Appendix A. Supplementary data

Supplementary data to this article can be found online at https://doi.org/10.1016/j.commatsci.2019.05.016.

References

[1] B. Gerald, Solid State Physics, Academic Press, New York, 1985.
[2] H. Yan, X. Wang, M. Yaon, X. Yao, Band structure design of semiconductors for enhanced photocatalytic activity: the case of TiO_2, Prog. Nat. Sci.: Mater. Int. 23 (2013) 402–407, https://doi.org/10.1016/j.pnsc.2013.06.002.
[3] M. Černá, M. Veselý, P. Dzik, Physical and chemical properties of titanium dioxide printed layers, Catal. Today 161 (2011) 97–104, https://doi.org/10.1016/j.cattod.2010.11.019.
[4] F. Mostaghni, Y. Abed, Structural, optical and photocatalytic properties of Co-TiO_2 prepared by sol-gel technique, Mater. Res. 19 (2016) 741–745 https://doi.org/doi:10.1590/1980-5373-mr-2016-0191.
[5] Z. Fu, Y.C. Liang, S.M. Wang, Z. Zhong, Structural phase transition and mechanical properties of TiO_2 under high pressure, Phys. Status Solidi B. 250 (2013) 2206–2214, https://doi.org/10.1002/pssb.201349186.
[6] P. Salvador, Analysis of the physical properties of TiO_2-Be electrodes in the photoassisted oxidation of water, Solar Energy Mater. 6 (1982) 241–250, https://doi.org/10.1016/0165-1633(82)90024-7.
[7] M. Kolář, H. Měšťánková, J. Jirkovský, M. Heyrovský, J. Šubrt, Some Aspects of physico-chemical properties of TiO_2 nanocolloids with respect to their age, size, and structure, Langmuir 22 (2006) 598–604, https://doi.org/10.1021/la058016w.
[8] M.A. Zhukovskiy, N.P. Smirnova, I.A. Rusetsky, G.Ya. Kolbasov, A.M. Eremenko, Physical and chemical properties and photocatalytic activity of nanostructured TiO_2/CdS films, J. Appl. Spectrosc. 81 (2014) 238–243, https://doi.org/10.1007/s10812-014-9916-7.
[9] T. Hoseinzadeh, Z. Ghorannevis, M. Ghoranneviss, A.H. Sari, M.K. Salem, Effects of various applied voltages on physical properties of TiO_2 nanotubes by anodization method, J. Theor. Appl. Phys. 11 (2017) 243–248, https://doi.org/10.1007/s40094-017-0257-9.
[10] T. Hoseinzadeh, Z. Ghorannevis, M. Ghoranneviss, M.K. Salem, A.H. Sari, Synthesis of different TiO_2 nanostructures and their physical properties, Chin. Phys. Lett. 34 (2017) 116101, , https://doi.org/10.1088/0256-307x/34/11/116101.
[11] M.H. Razali, M.N. Ahmad-Fauzi, A.R. Mohamed, S. Sreekantan, Physical properties study of TiO_2 nanoparticle synthesis via hydrothermal method using TiO_2 microparticles as precursor, Adv. Mater. Res. 772 (2013) 365–370, https://doi.org/10.4028/www.scientific.net/AMR.772.365.
[12] X. Rocquefelte, F. Goubin, H.J. Koo, M.H. Whangbo, S. Jobic, Investigation of the origin of the empirical relationship between refractive index and density on the basis of first principles calculations for the refractive indices of various TiO_2 phases, Inorg. Chem. 43 (2004) 2246–2251, https://doi.org/10.1021/ic035383r.
[13] X.G. Ma, P. Liang, L. Miao, S.W. Bie, C.K. Zhang, L. Xu, J.J. Jiang, Pressure-induced phase transition and elastic properties of TiO_2 polymorphs, Phys. Status Solidi B. 246 (2009) 2132–2139, https://doi.org/10.1002/pssb.200945111.
[14] X. Wu, E. Holbig, G. Steinle-Neumann, Structural stability of TiO2 at high pressure in density-functional theory based calculations, J. Phys.: Condens. Matter. 22 (2011) 295501, https://doi.org/10.1088/0953-8984/22/29/295501.
[15] J. Pascual, J. Camassel, H. Mathieu, Resolved quadrupolar transition in TiO_2, Phys. Rev. Lett. 39 (1977) 1490–1493, https://doi.org/10.1103/PhysRevLett. 39.1490.
[16] S.C. Abrahams, J.L. Bernstein, Rutile: normal probability plot analysis and accurate measurement of crystal structure, J. Chem. Phys. 55 (1971) 3206–3211, https://doi.org/10.1063/1.1676569.
[17] A. Fahmi, C. Minot, B. Silvi, M. Causá, Theoretical analysis of the structures of titanium dioxide crystals, Phys. Rev B. 47 (1993) 11717–11724, https://doi.org/10.1103/PhysRevB.47.11717.
[18] H.W. Peng, J.B. Li, S.S. Li, J.B. Xia, Possible origin of ferromagnetism in undoped anatase TiO_2, Phys. Rev B. 79 (2009) 092411, , https://doi.org/10.1103/PhysRevB.79.092411.
[19] B.L. Lee, X.Y. Wang, R. Bhave, M. Hu, Synthesis of brookite TiO_2 nanoparticles by ambient condition sol process, Mater. Lett. 60 (2006) 1179–1183, https://doi.org/10.1016/j.matlet.2005.10.114.
[20] R. Zallen, M.P. Moret, The optical absorption edge of brookite TiO_2, Solid State Commun. 137 (2006) 154–157, https://doi.org/10.1016/j.ssc.2005.10.024.
[21] M. Landmann, E. Rauls, W.G. Schmidt, The electronic structure and optical response of rutile, anatase and brookite TiO_2, J. Phys.: Condens. Matter 24 (2012) 195503, , https://doi.org/10.1088/0953-8984/24/19/195503.
[22] J.K. Burdett, T. Hughbanks, G.J. Miller, J.W. Richardson, J.V. Smith, Structural-electronic relationships in inorganic solids: powder neutron diffraction studies of the rutile and anatase polymorphs of titanium dioxide at 15K and 295K, J. Am. Chem. Soc. 109 (1987) 3639–3646, https://doi.org/10.1021/ja00246a021.
[23] S. Valencia, J.M. Marín, G. Restrepo, Study of the bandgap of synthesized titanium dioxide nanoparticules using the sol-gel method and a hydrothermal treatment, Open Mater. Sci. J. 4 (2010) 9–14, https://doi.org/10.2174/1874088X01004010009.
[24] R. Beranek, (Photo)electrochemical Methods for the Determination of the Band Edge Positions of TiO_2-Based Nanomaterials, Adv. Phys. Chem. 2011 (2011) 1–20, https://doi.org/10.1155/2011/786759.
[25] H. Gao, D. Zhang, M. Yang, S. Dong, Photocatalytic behavior of fluorinated rutile TiO_2 (110) surface: understanding from the band model, Solar RRL. 1 (2017) 1700183, https://doi.org/10.1002/solr.201700183.
[26] M. Janczarek, H. Kisch, J. Hupka, Photoelectrochemical characterization of nitrogen modified TiO_2, Physicochem. Probl. Miner. Process. 41 (2007) 159–166.
[27] M.S. Surinder, G. Nandini, material studies at high pressure. materials under extreme conditions: recent trends and future prospects, Elsevier (2017) 1–47, https://doi.org/10.1016/B978-0-12-801300-7.00001-2.
[28] M. Santoro, F. Gorelli, J. Haines, O. Cambon, C. Levelut, G. Garbarino, Silicon carbonate phase formed from carbon dioxide and silica under pressure, PNAS 108 (2011) 7689, https://doi.org/10.1073/pnas.1019691108.
[29] N. Garg, C. Murli, A.K. Tyagi, S.M. Sharma, Phase transitions in $Sc_2(WO_4)_3$ under high pressure, Phys. Rev B. 72 (2005) 064106, , https://doi.org/10.1103/PhysRevB.72.064106.
[30] W. Zhang, A.R. Oganov, A.F. Goncharov, Q. Zhu, S.E. Boulfelfel, A.O. Lyakhov, E. Stavrou, M. Somayazulu, V.P. Prakapenka, Z. Konôpková, Unexpected stable stoichiometries of sodium chlorides, Science 342 (2013) 1502–1505, https://doi.org/10.1126/science.1244989.
[31] H. Tups, K. Takemura, K. Syassen, Interband Optical Absorption and Electronic s – d Transition in Rb and Cs at High Pressures, Phys. Rev. Lett. 49 (1982) 1776–1779, https://doi.org/10.1103/PhysRevLett. 49.1776.
[32] T. Honda, T. Aoyama, J.S. White, T. Strassle, L. Keller, M. Kenzelmann, F. Honda, A. Miyake, K. Shimizu, Y. Wakabayashi, T. Kimura, Pressure effect on magnetism and multiferroicity in Mn_2GeO_4, Phys. Rev B. 89 (2014) 104405, , https://doi.org/10.1103/PhysRevB.89.104405.
[33] K.A. Goettel, J.H. Eggert, I.F. Silvera, W.C. Moss, Optical evidence for the metallization of xenon at 132(5) GPa, Phys. Rev. Lett. 62 (1989) 665–668, https://doi.org/10.1103/PhysRevLett. 62.665.
[34] T. Matsuoka, K. Shimizu, Direct observation of a pressure-induced metal-to-semiconductor transition in lithium, Nature 458 (2009) 186–189, https://doi.org/10.1038/nature07827.
[35] Y. Ma, M. Eremets, A.R. Oganov, Y. Xie, L. Trojan, S. Medvedev, A.O. Lyakhov, M. Valle, V. Prakapenka, Transparent dense sodium, Nature 458 (2009) 182–185, https://doi.org/10.1038/nature07786.
[36] B. Liu, Y. Han, C. Gao, Y. Ma, G. Peng, B. Wu, C. Liu, Y. Wang, T. Hu, X. Cui, W. Ren, Y. Li, N. Su, H. Liu, G. Zou, Pressure induced semiconductor-semimetal transition in WSe_2, J. Phys. Chem. C. 114 (2010) 14251–14254, https://doi.org/10.1021/jp104143e.
[37] B. Vasvari, A.O.E. Animalu, V. Heine, Electronic structure of Ca, Sr, and Ba under pressure, Phys. Rev. 154 (1967) 535–539, https://doi.org/10.1103/physrev.154.535.
[38] G. Kresse, J. Furthmüller, Efficient iterative schemes for ab initio total-energy calculations using a plane-wave basis set, Phys. Rev B. 54 (1996) 11169–11186, https://doi.org/10.1103/PhysRevB.54.11169.
[39] J.M. Soler, E. Artacho, J.D. Gale, A. Garcia, J. Junquera, P. Ordejon, D. Sanchez-Portal, The SIESTA Method for ab Initio Order-N Materials Simulation, J. Phys.: Condens. Matter. 14 (2002) 2745–2779, https://doi.org/10.1088/0953-8984/14/11/302.
[40] J.D. Gale, GULP: capabilities and prospects, Z. Kristallogr. 220 (2005) 552–554, https://doi.org/10.1524/zkri.220.5.552.65070.
[41] A.R. Oganov, C.W. Glass, Evolutionary crystal structure prediction as a tool in materials design, 064210 (6pp), J. Phys.: Condens. Matter. 20 (2008), https://doi.org/10.1088/0953-8984/20/6/064210.
[42] A.R. Oganov, S. Ono, Y. Ma, C.W. Glass, A. Garcia, Novel high-pressure structures of $MgCO_3$, $CaCO_3$ and CO_2 and their role in Earth's lower mantle, Earth Planet. Sci. Lett. 273 (2008) 38–47, https://doi.org/10.1016/j.epsl.2008.06.005.
[43] A.R. Oganov, C.W. Glass, Crystal structure prediction using ab initio evolutionary techniques: principles and applications, J. Chem. Phys. 124 (2006) 244704, , https://doi.org/10.1063/1.2210932.
[44] C.W. Glass, A.R. Oganov, N. Hansen, USPEX—Evolutionary crystal structure prediction, Comp. Phys. Comm. 175 (2006) 713–720, https://doi.org/10.1016/j.cpc.2006.07.020.
[45] A.O. Lyakhov, A.R. Oganov, M. Valle, How to predict very large and complex crystal structures, Comp. Phys. Commun. 181 (2010) 1623–1632, https://doi.org/10.1016/j.cpc.2010.06.007.
[46] A.O. Lyakhov, A.R. Oganov, H.T. Stokes, Q. Zhu, New developments in evolutionary structure prediction algorithm USPEX, Comp. Phys. Comm. 184 (2013) 1172–1182, https://doi.org/10.1016/j.cpc.2012.12.009.
[47] A.R. Oganov, A.O. Lyakhov, M. Valle, How evolutionary crystal structure prediction works—and why, Acc. Chem. Res. 44 (2011) 227–237, https://doi.org/10.1021/ar1001318.
[48] P. Hohenberg, W. Kohn, Inhomogeneous electron gas, Phys Rev. 136 (1964) B864–B871, https://doi.org/10.1103/PhysRev. 136.B864.
[49] W. Kohn, L.J. Sham, Self-consistent equations including exchange and correlation effects, Phys Rev. 140 (1965) A1133–A1138, https://doi.org/10.1103/PhysRev.140.A1133.
[50] J.P. Perdew, K. Burke, M. Ernzerhof, Generalized gradient approximation made simple, Phys. Rev. Lett. 77 (1996) 3865–3868, https://doi.org/10.1103/PhysRevLett. 77.3865.
[51] P.E. Blöchl, Projector augmented-wave method, Phys. Rev. B. 50 (1994) 17953–17979, https://doi.org/10.1103/PhysRevB.50.17953.
[52] G. Kresse, D. Joubert, From ultrasoft pseudopotentials to the projector augmented-wave method, Phys. Rev. B. 59 (1999) 1758–1775, https://doi.org/10.1103/PhysRevB.59.1758.
[53] G. Kresse, J. Hafner, Ab initio molecular dynamics for liquid metals, Phys. Rev. B. 47 (1993) 558–561, https://doi.org/10.1103/PhysRevB.47.558.
[54] G. Kresse, J. Hafner, Ab initio molecular-dynamics simulation of the liquid-metal–amorphous-semiconductor transition in germanium, Phys. Rev. 49 (1994) 14251–14269, https://doi.org/10.1103/PhysRevB.49.14251.

[55] A. Bilić, J.D. Gale, M.A. Gibson, N. Wilson, K. McGregor, Prediction of novel alloy phases of Al with Sc or Ta, Sci. Rep. 5 (2015) 9909, https://doi.org/10.1038/srep09909.
[56] L. Wang, Relationship between Intrinsic Breakdown Field and Bandgap of Materials, 2006 25th International Conference on Microelectronics, 2006, pp. 576–579, , https://doi.org/10.1109/ICMEL.2006.1651032.
[57] M. Ieong, B. Doris, J. Kedzierski, K. Rim, M. Yang, Silicon device scaling to the sub-10-nm regime, Science 306 (2004) 2057–2060, https://doi.org/10.1126/science.1100731.
[58] Q. Zeng, A.R. Oganov, A.O. Lyakhov, C. Xie, X. Zhang, J. Zhang, Q. Zhu, B. Wei, I. Grigorenko, L. Zhanga, L. Chenga, Evolutionary search for new high-k dielectric materials: methodology and applications to hafnia-based oxides, Acta Cryst C. 70 (2014) 76–84, https://doi.org/10.1107/S2053229613027861.
[59] A. Togo, I. Tanaka, First principles phonon calculations in materials science, Scr. Mater. 108 (2015) 1–5, https://doi.org/10.1016/j.scriptamat.2015.07.021.
[60] S.J. Clark, M.D. Segall, C.J. Pickard, P.J. Hasnip, M.J. Probert, K. Refson, M.C. Payne, First principles methods using CASTEP, Zeitschrift fuer Kristallographie. 220 (2005) 567–570, https://doi.org/10.1524/zkri.220.5.567.65075.
[61] K. Momma, F. Izumi, VESTA 3 for three-dimensional visualization of crystal, volumetric and morphology data, J. Appl. Crystallogr. 44 (2011) 1272–1276, https://doi.org/10.1107/S0021889811038970.
[62] E. Seifert, OriginPro 9.1: scientific data analysis and graphing software-software review, 1552–1552, J. Chem. Inf. Model. 54 (2014), https://doi.org/10.1021/ci500161d.
[63] D. Adler, H. Brooks, Theory of semiconductor-to-metal transitions physical review, Phys. Rev. 155 (1967) 826–840, https://doi.org/10.1103/PhysRev. 155.826.
[64] T.P. Feist, P.K. Davies, The soft chemical synthesis of TiO_2 (B) from layered titanates, J. Solid State Chem. 101 (1992) 275–295, https://doi.org/10.1016/0022-4596(92)90184-W.
[65] A. Jain, S.P. Ong, G. Hautier, W. Chen, W.D. Richards, S. Dacek, S. Cholia, D. Gunter, D. Skinner, G. Ceder, K.A. Persson, Commentary: The Materials Project: a materials genome approach to accelerating materials innovation, APL Mater. 1 (2013) 011002, , https://doi.org/10.1063/1.4812323.
[66] H. Dekura, T. Tsuchiya, Y. Kuwayama, J. Tsuchiya, Theoretical and Experimental Evidence for a New Post-Cotunnite Phase of Titanium Dioxide with Significant Optical Absorption, Phys. Rev. Lett. 107 (2011), https://doi.org/10.1103/PhysRevLett. 107.045701.
[67] X. Zhong, J. Wang, S. Zhang, G. Yang, Y. Wang, Ten-fold coordinated polymorph and metallization of TiO_2 under high pressure, RSC. Adv. 5 (2015) 54253–54257, https://doi.org/10.1039/c5ra07245j.
[68] M.J. Lylea, C.J. Pickardb, R.J. Needsa, Prediction of 10-fold coordinated TiO_2 and SiO_2 structures at multimegabar pressures, PNAS 112 (2015) 6898–6901, https://doi.org/10.1073/pnas.1500604112.
[69] J. Muscat, V. Swamy, N.M. Harrison, First-principles calculations of the phase stability of TiO_2, Phys. Rev. B. 65 (2002) 224112, , https://doi.org/10.1103/PhysRevB.65.224112.
[70] H.B. Schlegel, Optimization of equilibrium geometries and transition structures, J. Comput. Chem. 3 (1982) 214–218, https://doi.org/10.1002/jcc.540030212.
[71] O.L. Anderson, Equations of State of Solids for Geophysics and Ceramic Science, Oxford University Press, Oxford, 1995, p. 405.
[72] L.C. Ming, M.H. Manghnani, Isothermal Compression of TiO_2 (Rutile) Under Hydrostatic Pressure to 106 kbar, J. Geophys. Res. 84 (1979) 4777–4779, https://doi.org/10.1029/JB084iB09p04777.
[73] Y. Al-Khatatbeh, K.K.M. Lee, B. Kiefer, High-pressure behavior of TiO_2 as determined by experiment and theory, Phys. Rev. B. 79 (2009) 134114, , https://doi.org/10.1103/PhysRevB.79.134114.
[74] V. Swamy, B.C. Muddle, Ultrastiff cubic TiO_2 identified via first-principles calculations, Phys. Rev. Lett. 98 (2007) 035502, , https://doi.org/10.1103/PhysRevLett.98.035502.
[75] M. Iuga, G. Steinle-Neumann, J. Meinhardt, Ab-initio simulation of elastic constants for some ceramic materials, Eur. Phys. J. B. 58 (2007) 127–133, https://doi.org/10.1140/epjb/e2007-00209-1.
[76] M. Mikami, S. Nakamura, O. Kitao, H. Arakawa, X. Gonze, First-principles study of titanium dioxide: rutile and anatase, Jpn. J. Appl. Phys. 39 (2000) L 847–L 850, https://doi.org/10.1143/JJAP.39.L847.
[77] M.E. Arroyo-de Dompablo, A. Morales-García, M. Taravillo, DFT + U calculations of crystal lattice, electronic structure, and phase stability under pressure of TiO_2 polymorphs, J. Chem. Phys. 135 (2011) 054503, https://doi.org/10.1063/1.3617244.
[78] C. Lu, C. Chen, High-pressure evolution of crystal bonding structures and properties of FeOOH, J. Phys. Chem. Lett. 9 (2018) 2181–2185, https://doi.org/10.1021/acs.jpclett.8b00947.
[79] C. Lu, M. Amsler, C. Chen, Unraveling the structure and bonding evolution of the newly discovered iron oxide FeO_2, 054102, Phys. Rev. B. 98 (2018), https://doi.org/10.1103/physrevb.98.054102.
[80] W. Zhou, N. Umezawa, R. Ma, N. Sakai, Y. Ebina, K. Sano, M. Liu, Y. Ishida, T. Aida, T. Sasaki, Spontaneous direct band-gap, high hole mobility and huge exciton energy in atomic-thin TiO2 nanosheet, Chem. Mater. 30 (2018) 6449–6457, https://doi.org/10.1021/acs.chemmater.8b02792.